Ann. Geophys., 27, 2027–2034, 2009
www.ann-geophys.net/27/2027/2009/

Annales Geophysicae

Equinoctial asymmetry of a low-latitude ionosphere-thermosphere system and equatorial irregularities: evidence for meridional wind control

T. Maruyama[1], **S. Saito**[1,*], **M. Kawamura**[1], **K. Nozaki**[1,**], **J. Krall**[2], **and J. D. Huba**[2]

[1]National Inst. of Information and Communications Technology, 2-1 Nukui-kita 4-chome, Koganei, Tokyo 184-8795, Japan
[2]Plasma Physics Division, Naval Research Lab., Code 6790, 4555 Overlook Ave., SW, Washington, D.C., 20375-5000, USA
[*]now at: Electric Navigation Research Institute, 42-23 Jindaiji-Higashi 7-chome, Chofu, Tokyo 182-0012, Japan
[**]now at: Telecom Engineering Center, 7-2 Yashio 5-chome, Shinagawa-ku, Tokyo 140-0003, Japan

Received: 1 October 2008 – Revised: 8 April 2009 – Accepted: 8 April 2009 – Published: 4 May 2009

Abstract. Nocturnal ionospheric height variations were analyzed along the meridian of 100° E by using ionosonde data. Two ionosondes were installed near the magnetic conjugate points at low latitudes, and the third station was situated near the magnetic equator. Ionospheric virtual heights were scaled every 15 min and vertical $\boldsymbol{E}\times\boldsymbol{B}$ drift velocities were inferred from the equatorial station. By incorporating the inferred equatorial vertical drift velocity, ionospheric bottom heights with the absence of wind were modeled for the two low-latitude conjugate stations, and the deviation in heights from the model outputs was used to infer the transequatorial meridional thermospheric winds. The results obtained for the September and March equinoxes of years 2004 and 2005, respectively, were compared, and a significant difference in the meridional wind was found. An oscillation with a period of approximately 7 h of the meridional wind existed in both the equinoxes, but its amplitude was larger in September as compared to that in March. When the equatorial height reached the maximum level due to the evening enhancement of the zonal electric field, the transequatorial meridional wind velocity reached approximately 10 and 40 m/s for the March and September equinoxes, respectively. This asymmetry of the ionosphere-thermosphere system was found to be associated with the previously reported equinoctial asymmetry of equatorial ionospheric irregularities; the probability for equatorial irregularities to occur is higher in March as compared to that in September at the Indian to Western Pacific longitudes. Numerical simulations of plasma bubble developments were conducted by incorporating the transequatorial neutral wind effect, and the results showed that the growth time (e-folding time) of the bubble was halved when the wind velocity changed from 10 to 40 m/s.

Keywords. Ionosphere (Ionosphere-atmosphere interactions; Ionospheric irregularities) – Meteorology and atmospheric dynamics (Thermospheric dynamics)

1 Introduction

A distinctive feature of equatorial spread F (ESF) or plasma bubbles is the seasonal-longitudinal occurrence pattern. The zonal mean activity of ESF peaks at equinoxes, and the season of ESF shifts towards the December solstice at the Atlantic longitudes and towards the June solstice at the Pacific longitudes (Maruyama and Matuura, 1984; Burke et al., 2004). The longitudes are characterized by the magnetic declination angle, i.e., the largely westward and eastward magnetic declinations at the Atlantic and Pacific longitudes, respectively. The coupled seasonal and longitudinal effect of ESF and its connection with the magnetic declination angle has led to hypotheses about the control mechanisms for ESF and plasma bubble onsets (Maruyama and Matuura, 1984; Tsunoda, 1985). The basic mechanism for ESF and plasma bubble onsets is the Rayleigh-Taylor instability. Maruyama and Matuura (1984) ascribed the seasonal-longitudinal control of ESF occurrence to the modification of the growth rate for the Rayleigh-Taylor instability through

Correspondence to: T. Maruyama
(tmaru@nict.go.jp)

Published by Copernicus Publications on behalf of the European Geosciences Union.

the transequatorial component of thermospheric winds in the magnetic meridional plane. Tsunoda (1985) ascribed the seasonal-longitudinal control of ESF occurrence to the alignment of the magnetic meridional plane and the sunset terminator line, which determines the E-region sunset times at the conjugate points and causes the current convective instability.

Both the hypotheses described above address the climatology of the seasonal/longitudinal effect of ESF. Mendillo et al. (1992) examined the meridional wind control of the Rayleigh-Taylor instability to explain the day-to-day variability of ESF. They compared the observations on two nights. The major difference between nights when ESF instabilities did not occur and did occur is that the northern meridional gradient of 630-nm airglow was reduced, which was attributed to the equatorward neutral winds, on the night with limited ESF activity. Later, Mendillo et al. (2001) examined the data obtained during the Multi-Instrumented Studies of Equatorial Thermospheric Aeronomy (MISETA) campaign and found no convincing evidence for the wind suppression mechanism. Valladares et al. (2004a, b) concluded that the meridional wind may not be able to inhibit the growth of ESF irregularities. On the other hand, Saito and Maruyama (2006) demonstrated, through case studies of data obtained from a meridional ionosonde network, that even when $h'F$ at the equatorial station was largely enhanced, plasma bubbles were not generated when $h'F$ at low latitudes possessed a noticeable north/south asymmetry. Thampi et al. (2006, 2008) have shown that the north/south asymmetry of total electron content at the equatorial anomaly crests could be related with the absence of ESF, although the asymmetry alone does not suffice to make a deterministic forecast for ESF on a given day. Thus, regarding the meridional wind suppression of ESF, there still remain uncertainties that must be investigated.

Burke et al. (2004) generated a comprehensive global distribution map (longitude vs. season) of equatorial ionospheric irregularities on the basis of the Defense Meteorological Satellite Program (DMSP) in-situ observations. The map indicates high occurrence probabilities along two lines around the equinox seasons, where the sunset terminator aligns with the magnetic meridional plane. Another feature noted in the map is the equinoctial asymmetry, although it is not as prominent as the seasonal change and longitudinal peculiarity. At the Indian to Western Pacific longitudes, the maximum occurrence probability around the March equinox is higher than that around the September equinox. On the other hand, at the longitudes of the Eastern-Pacific Ocean, the maximum occurrence probability around the September equinox is higher than that around the March equinox. Ground-based observations of the same equinoctial asymmetry of ionospheric irregularities are reported on the basis of scintillation measurements at the Indian and Southeast Asian longitudes (Otsuka et al., 2006; Ogawa et al., 2006; Ray and DasGupta, 2007), off-great-circle propagation of transequatorial high frequency (HF) waves at the Western Pacific longitudes (Maruyama and Kawamura, 2006), and optical measurements at the Hawaiian longitudes (Kim et al., 2002; Makela et al., 2004). If the ionosphere-thermosphere system and plasma bubble occurrence are directly controlled by the angle between the sunset terminator line and magnetic meridian, the March and September equinoxes would exhibit similar bubble morphology because the geometry between the earth and the sun is the same at the two equinoxes. The equinoctial asymmetry of ESF occurrence, which might not be as intense as other morphological features such as the seasonal-longitudinal effect, is a key to testing possible controlling mechanisms for plasma bubble onsets. This paper focuses on a discussion on the observed equinoctial asymmetry of the equatorial ionosphere-thermosphere system by using data obtained from a meridional ionosonde network in Southeast Asia, irregularities at the same longitude, and numerical simulations of plasma bubble developments.

2 Observations

Multipoint ionosonde observation was conducted along the 100° E meridian in the Southeast Asia low-latitude ionospheric network (SEALION) (Maruyama et al., 2007). Two ionosondes were installed near the magnetic conjugate points at Chiang Mai, Thailand (18.8° N, 98.9° E; 13.0° magnetic latitude) and Kototabang, Indonesia (0.2° S, 100.3° E; −10.0° magnetic latitude), and the third ionosonde was installed near the magnetic equator at Chumphon, Thailand (10.7° N, 99.4° E; 3.3° magnetic latitude), as shown in Fig. 1. By using data obtained from a meridional ionosonde chain, thermospheric meridional winds were estimated. For this purpose, virtual heights at the three stations were scaled and median values were evaluated for two one-month periods centered on the equinoxes: 8 September–8 October 2004 and 5 March–4 April 2005; these periods are referred to as September 2004 and March 2005, respectively, in the remaining sections of this paper. Considering the median values has the advantage of reducing the possible effects of anomalous changes caused by magnetic disturbances.

At low latitudes, equatorward winds push up the ionosphere to higher altitudes, and poleward winds depress it to lower altitudes. Therefore, the height difference between the two conjugate stations is related to the transequatorial meridional wind. However, ionospheric heights are also affected by zonal electric fields that drive the ionosphere in the vertical $\boldsymbol{E}\times\boldsymbol{B}$ direction. To derive the meridional wind, the same method described by Maruyama et al. (2008) was employed, as follows:

– At the magnetic equator, the wind effect on the changes in height is reduced and the $\boldsymbol{E}\times\boldsymbol{B}$ drift effect is maximized. The $\boldsymbol{E}\times\boldsymbol{B}$ drift was estimated by using modeling calculations in which the $\boldsymbol{E}\times\boldsymbol{B}$ drift pattern was adjusted so that the modeled height for an electron density

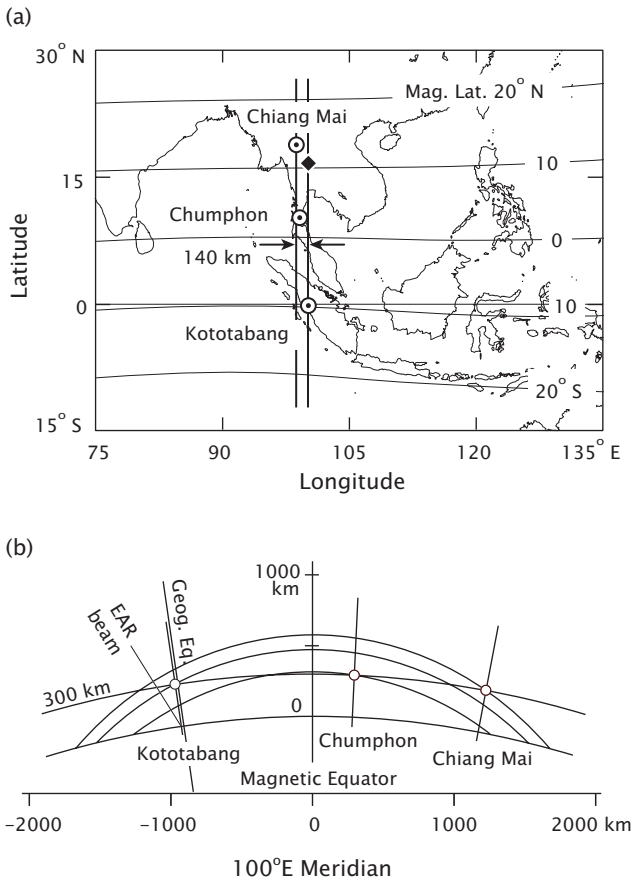

Fig. 1. **(a)** Locations of the three ionosondes of SEALION, and **(b)** magnetic field lines passing 300 km above each ionosonde along the 100° E meridian. The beam direction of the EAR (Equatorial Atmosphere Radar) for field aligned irregularity observation is overlaid in panel (b).

of 7.75×10^{10} m^{-3} corresponds with the observations on $h'F$ at 2.5 MHz over Chumphon.

- The modeled ionospheric heights at the low-latitude stations without the thermospheric wind effect were obtained by incorporating the $\boldsymbol{E}\times\boldsymbol{B}$ drift velocity obtained above.
- The difference between the observed and no-wind model heights ($\Delta h'F$) were used to estimate the meridional wind.
- The double differential between Kototabang (KT) and Chiang Mai (CM), ($\Delta h'F$(KT) – $\Delta h'F$(CM)), was a suitable proxy for the transequatorial meridional wind (with respect to the magnetic equator).

Figure 2 shows the double differential of height deviations calculated for September 2004 and March 2005. The local solar time (true solar time) is taken in the abscissa so that the sunset times for the two periods coincide. For reference,

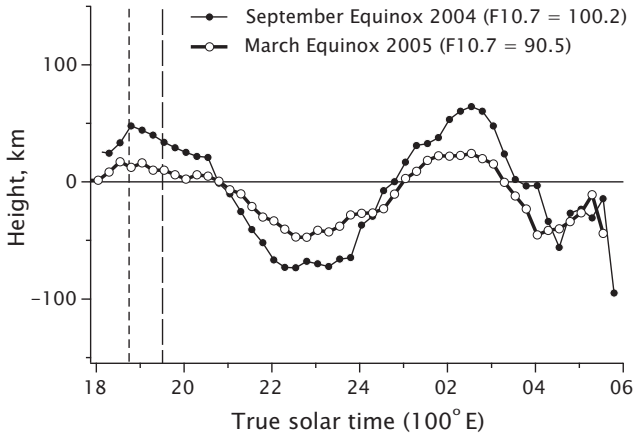

Fig. 2. Double differentials of height deviation from the no-wind reference at the conjugate points for one-month periods centered on the equinoxes of September 2004 and March 2005. Height in km is read as wind velocity in m/s, and the positive sign corresponds to the northward direction.

the vertical short-dashed line corresponds to the sunset at the E-region height (120 km), and the long-dashed line corresponds to the sunset at 520 km above the magnetic equator, based upon the fact that most plasma bubble onsets are observed near the sunset at 520 km above the magnetic equator by the Equatorial Atmosphere Radar (EAR) at Kototabang (see Fig. 1) (Yokoyama et al., 2004). The double differentials, and thus the meridional winds (positive northward), oscillated with a period of approximately 7 h during both the equinoxes, and the amplitude was larger in September as compared to that in March. (Note that the data obtained during the periods before 18:30 LST and after 04:00 LST are not very accurate because the $h'F$ was affected by ionization at lower altitudes and the small *fo*F2 values).

Figure 3 shows the height variations over Chumphon for the same periods as those in Fig. 2. The maximum heights and their times during evening hours caused by the prereversal enhancement of the eastward electric field were almost the same for both the equinoxes, but the succeeding layer descent was faster in September 2004 as compared to that in March 2005.

3 Discussion

3.1 Equinox asymmetry

As presented in Figs. 2 and 3, the dynamics of the low-latitude ionosphere-thermosphere system was not symmetric for the March and September equinoxes. Another equinoctial asymmetry is known to exist for the equatorial irregularities (Kim et al., 2002; Makela et al., 2004; Maruyama and Kawamura, 2006; Otsuka et al., 2006; Ray and DasGupta, 2007). Ogawa et al. (2006) and Otsuka et al. (2006) observed

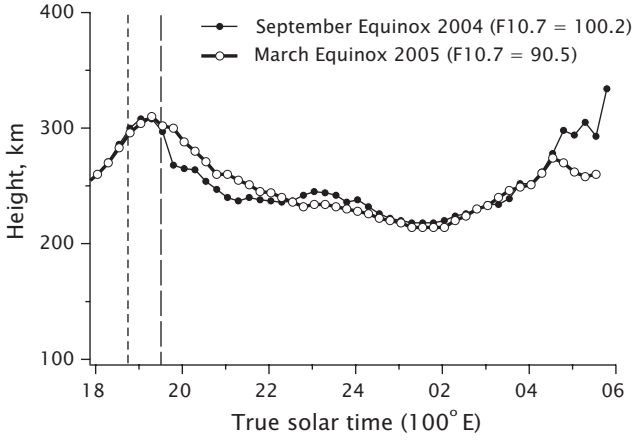

Fig. 3. Equatorial height variations over Chumphon for the same period as that in Fig. 2.

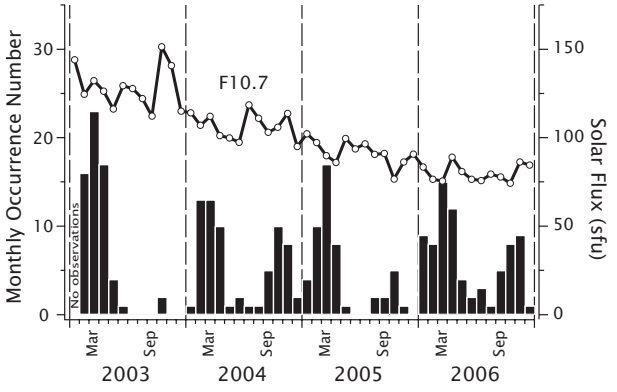

Fig. 4. Off-great-circle propagation of transequatorial HF waves between Australia and Japan, which is related to the formation of equatorial spread F (Kelleher and Röttger, 1973; Röttger, 1976).

a seasonal variation in equatorial irregularities with scintillations of GPS signals at 1.6 GHz at Kototabang (the same location as one of the SEALION ionosondes) over a period of two years during the descending phase of the solar activity. Scintillations at high frequencies, such as those of GPS radio signals, are known to be caused by plasma bubbles. In addition, Fig. 4 shows a longer period of observations of off-great-circle propagation of transequatorial HF waves between Australia and Japan; this is an extension of the similar figure shown by Maruyama and Kawamura (2006). The off-great-circle propagation is caused by large-scale structures near the magnetic equator that are associated with the formation of equatorial spread F (Kelleher and Röttger, 1973; Röttger, 1976). The equinoctial asymmetry was observed every year, although the degree of the asymmetry varied from year to year. The figure indicates that the equinoctial asymmetry was not an apparent effect caused by decreasing the solar activity. Ray and DasGupta (2007) observed the same equinoctial asymmetry of 1.5-GHz scintillations at the Indian longitude during the solar ascending phase; they ascribed the equinoctial asymmetry to the difference in the ambient ionization between the two equinoxes, because scintillations depend on the amplitude of the irregularities. However, the equinoctial asymmetry of off-great-circle propagation events of transequatorial HF waves and optical measurments (Kim et al., 2002; Makela et al., 2004) may not have been affected by the ambient electron density. Thus, the equinoctial asymmetry of the equatorial irregularities must be a true effect.

The basic mechanism of plasma bubble generation is the gravitational Rayleigh-Taylor instability operating on the bottomside of the F-layer. The growth rate of the instability increases when the layer height is high, which causes the ion-neutral collision frequency to be low. In addition to the gravitational term, eastward electric fields directly destabilize the ionosphere. Thus, the enhancement of the eastward electric field after sunset, caused by the F-region dynamo (evening enhancement), is a leading factor that affects the bubble onsets. However, Abdu (2001) asserted that the vertical drift alone is not sufficient to describe the onsets of plasma bubbles. Another factor is the amount of Pedersen conductivity at low latitudes apart from the equator, where the perturbation electric field of the instability process is mapped along magnetic field lines. The transequatorial wind that increases the field line integrated Pedersen conductivity was proposed as a suppression mechanism of the instability (Maruyama and Matuura, 1984; Maruyama, 1988; Saito and Maruyama, 2006). In addition to the Pedersen conductivity term, a meridional wind component perpendicular to the magnetic field line was shown to suppress the instability growth rate (Zalesak and Huba, 1991; Krall et al., 2009).

The ambient ionosphere-thermosphere conditions during the period between the E-region sunset and the most probable onset time, as discussed below, would strongly control the onsets of plasma bubbles. Yokoyama et al. (2004) observed VHF coherent echoes from field-aligned irregularities associated with plasma bubbles by using the EAR at Kototabang (20° magnetic dip angle, see Fig. 1). The EAR is a beam-steerable radar that can snapshoot echoing regions, unlike the slit-camera technique. Thus, the echoing regions can be distinguished if they appear in the observing beam area or are moved in from outside. The authors observed that most plasma bubbles were generated near the time of sunset at the equatorial heights mapped from the EAR echoing region along the magnetic field line. The equatorial height corresponding to the EAR echoing region at a height of 300 km was approximately 520 km. This sunset time is represented by the long-dashed line in Figs. 2 and 3, being slightly behind the time when the layer reached the maximum heights (Fig. 3). The leading time, during which geophysical noises or seeds are linearly developed, is considered necessary for the onsets of plasma bubbles. However, before the E-region sunset, the linear growth rate for the instability is small because of the high Pedersen conductivity at the E-layer heights

connected to the bottom of the F region by magnetic field lines. Thus, the most important time slot lies between the short-dashed and long-dashed lines shown in Figs. 2 and 3, and it is referred to as a leading slot.

Previous numerical modeling attempts (Maruyama et al., 2008) have shown that the 50-km double differential in Fig. 2 corresponds approximately to 50-m/s meridional wind for the particular geometry of SEALION. The wind direction oscillated in both the two equinoctial periods with very similar phases and periods. However, the amplitude of the wind oscillation in March 2005 was only half that of the oscillation in September 2004. As a result, the northward wind velocity during the leading slot in September was 3-4 times larger than that in March. Larger transequatorial meridional winds and the smaller probability of equatorial irregularity occurrence in September were qualitatively consistent with the scenario where the transequatorial neutral winds suppress the Rayleigh-Taylor instability.

3.2 Origin of the wind variation

Although our interest is focused on the meridional wind in the leading slot when plasma bubbles are generated, the wind dynamics should be discussed for wider local times for a comprehensive understanding of the phenomena, as the nocturnal wind shown in Fig. 2 systematically varies through the night. Meriwether et al. (2008) observed nightly variations of thermospheric winds and temperatures with high accuracy at a low-latitude station Arequipa, Peru (16.4° S, 71.4° W), which allowed to draw local time-latitude maps of horizontal wind. In the late winter to spring season of the Southern Hemisphere (e.g., the bottom panel of Fig. 7 of Meriwether et al., 2008), the wind is directed poleward during the early evening hours, followed by the equatorward surge immediately before midnight, and then it is reversed poleward again.. The periodic change in the wind direction is consistent with that represented in Fig. 2 in this paper. More importantly, the horizontal wind maps reveal the anti-cyclonic behavior of the wind vector showing equatorward flow followed by a rotation poleward within ∼4 h, which is consistent with the behavior of a terdiurnal tidal wave (Meriwether et al., 2008). Thus, our meridional wind/plasma bubble onset characteristics presumably reflect the climatology of tidal behavior.

Another interesting observation that might be connected with the current analysis is thermospheric density perturbations measured by the CHAMP satellite. Forbes et al. (2008) analyzed the ratio of the high-pass filtered densities to the trend that is removed (relative residual densities). Global maps of relative residual density contours in a local time vs. latitude frame revealed distinctive density perturbations in daytime and nighttime. The nighttime pattern showed a banded structure inclined at approximately 30° with respect to the dusk terminator at equatorial to mid-latitudes. The density enhanced band formed a V (or inverted V) shape open from the equator toward the winter hemisphere centered at midnight (the band after midnight appeared to incline at approximately 30° with respect to the dawn terminator). At low latitudes around 10° N, nocturnal variation in the relative residual densities exhibited a single peak near midnight in northern summer and showed two peaks separated by ∼4 h in northern winter. Maruyama et al. (2008) derived seasonal variations in the mean meridional wind between 0° and 18.8° N from the SEALION ionosonde observations. In northern summer, the nocturnal equatorward wind (directed from summer to winter hemisphere) forms a single peak with the maximum at around 23:00 LT. Whereas, in northern winter, the nocturnal poleward wind (directed from summer to winter again) peaks twice in the early evening and after midnight. Thus, there is a morphological resemblance between the two observations, the relative residual densities and the meridional winds determined from ionosonde observations. The equinoctial meridional winds depicted in Fig. 2 show the transitional behavior between summer and winter (Maruyama et al., 2008), and they are expected to be related with the relative density residual, although maps are not shown in Forbes et al. (2008). The observed relative residual density variations were termed the solar terminator wave (Forbes et al., 2008), and the terminator wave feature is reproduced by the Kyushu general circulation model (GCM) extending from the ground surface including the surface topography and land-sea contrast to the exobase (Miyoshi and Fujiwara, 2008). By examining the GCM outputs and the relative residual density maps, Forbes et al. (2008) suggest that the terminator wave is partially driven in-situ and that it is the result of excitation at lower altitudes and transmission upwards as a spectrum of waves.

All the three observations by Meriwether et al. (2008), Forbes et al. (2008), and Maruyama et al. (2008) with different techniques are consistent and suggest that the meridional winds discussed in the study might be forced from the lower atmosphere. The origin of the equinoctial asymmetry of thermospheric winds is not clear, and the longitudinal variations in the asymmetry feature of the winds are unknown unlike the morphology of ionospheric irregularities, either. However, the equinoctial asymmetry of the winds likely results from the lower atmosphere and the surface topography. A connection of wind variations with the midnight temperature maximum is addressed in the above three studies; Meriwether et al. (2008) demonstrate the development of an equatorward surge prior to the onset of MTM events with the horizontal wind maps, and other studies discuss the published MTM morphology (Herrero and Spencer, 1982). However, it is not clear if the wind variation in the leading slot of plasma bubble onset or early evening hours is directly connected with the MTM formation, even if they have a common origin.

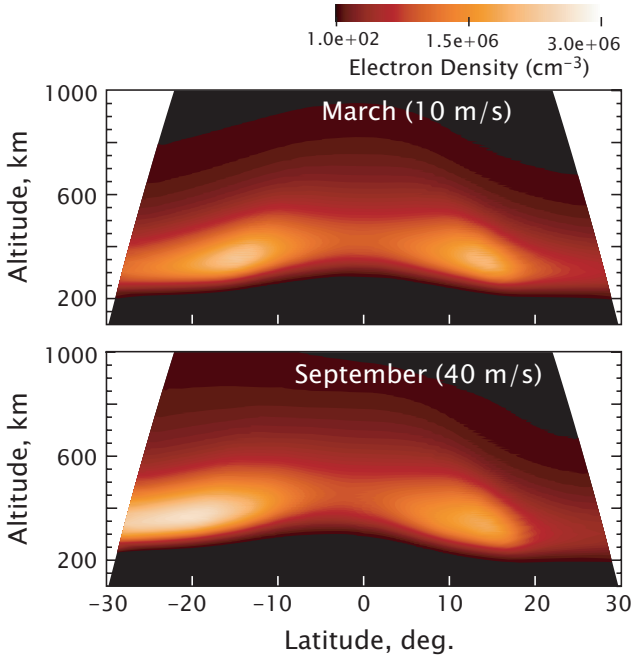

Fig. 5. Contours of electron density plotted in the latitude-altitude plane for the 10-m/s (upper panel) and 40-m/s (lower panel) cases. These show the initial states before ESF develops.

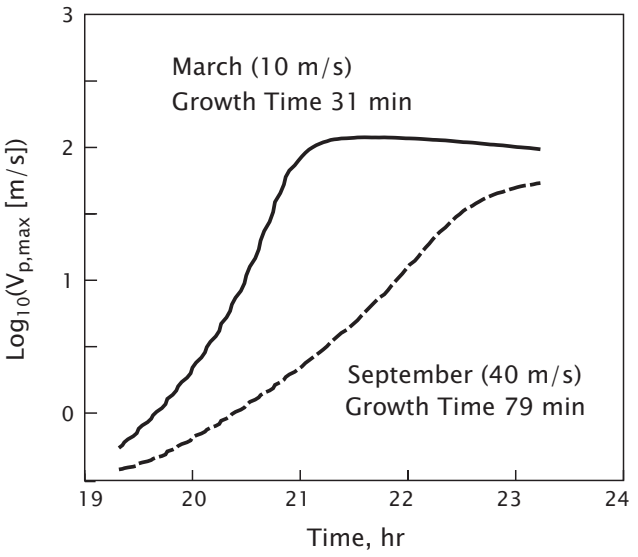

Fig. 6. Time evolution of upward bubble velocity for the two cases, corresponding to the equinoxes for September 2004 and March 2005.

3.3 Numerical simulations

To confirm whether a 40-m/s wind velocity is sufficient to suppress the instability growth, numerical simulations were conducted. A modified version of the NRL 3-D global ionosphere code SAMI3 (Huba et al., 2000, 2005) was used for this purpose. This version of SAMI3 was recently applied to ESF studies (Huba et al., 2008; Krall et al., 2009) and models a "wedge" of the post-sunset ionosphere; it was limited to 4° in longitude with a periodic boundary condition in order to obtain sufficient resolution for ESF modeling. Further, the perpendicular electric field $\boldsymbol{E}_{\perp}=-\nabla\,\Phi$ was determined self-consistently to calculate the $\boldsymbol{E}\times\boldsymbol{B}$ drifts.

The SAMI3 code, which is based on the 2-D ionosphere model SAMI2 (Huba et al., 2000), models the plasma and chemical evolution of seven ion species (H^+, He^+, N^+, O^+, N_2^+, NO^+, and O_2^+). The complete ion temperature equation is solved for three ion species (H^+, He^+, and O^+) as well as the electron temperature equation. Ion inertia is included in the ion momentum equation for motion along the geomagnetic field line, and $\boldsymbol{E}\times\boldsymbol{B}$ drifts are computed to obtain motion transverse to the magnetic field. The neutral composition and temperature are specified by using the empirical NRLMSISE00 model (Picone et al., 2002). For simplicity, this version of SAMI3 uses a non-tilted dipole for the model geomagnetic field. The simulations include the effect of a constant meridional wind (all other winds are set to zero) both in terms of the effect of the redistributed plasma on the field-line integrated conductivities (Maruyama, 1988) and the effect of the wind component perpendicular to the magnetic field (Zalesak and Huba, 1991; Krall et al., 2009).

Two cases were simulated. In one case the meridional wind speed was set to u_m=40 m/s, as discussed above; F10.7=F10.7A=100.2; and the day of year was set to 263, corresponding to the 2004 September equinox observations. In the other case, the wind speed was set to u_m=10 m/s; F10.7=F10.7A=90.5; and the day of year was set to 80, corresponding to the 2005 March equinox observations. In both the cases A_p=4, and the geographic longitude was set to 0° so that the universal and local times were identical in the simulations. The solar activity described by F10.7 enters into SAMI3/ESF calculations through ionization of the background and through the initial height of the F layer; the initial F-layer height was determined by an empirical $\boldsymbol{E}\times\boldsymbol{B}$ drift model (Scherliess and Fejer, 1999) in the SAMI2 calculation of the initial condition. As a result of the northward wind, the southern ionosphere was pushed upwards and the conjugate northern ionosphere was pushed downwards. This is illustrated in Fig. 5 in the latitude-altitude plane for the 10-m/s, F10.7=90.5 case (upper panel) and for the 40-m/s, F10.7=100.2 case (lower panel). The effect was clearly stronger for the 40 m/s case. For ESF simulations, a rather large Gaussian-like perturbation in the ion density was imposed at the beginning of each simulation (at 19:15 UT): a peak ion density perturbation of 25% centered at 2° longitude with a half-width of 0.25° and at an altitude z=300 km with a half-width of 60 km.

As in study of Krall et al. (2009), the growth times are determined from the peak upward drift velocity $V_{p,\max}$ during the linear phase of the instability. Plots of $\log_{10}(V_{p,\max})$

are shown in Fig. 6 for the March (solid line) and September (dashed line) cases. We attribute the wiggles in the March curve to the large initial perturbation; they were not present when a milder perturbation was used. The instability grew slowly in the September case, with the upward $\boldsymbol{E}\times\boldsymbol{B}$ drift velocity barely exceeding 10 m/s within the first two hours of the simulation. In the March case, the upward drift velocity exceeded 300 m/s, and the ESF bubbles rose to an altitude of approximately 1100 km by the end of the 4-h simulation period (19:15–23:15 UT). Consistent with past results (Huba et al., 2008; Krall et al., 2009), the peak plasma drift velocity (∼350 m/s) exceeded the peak bubble velocity (∼80 m/s) during the non-linear phase of the instability. The initial growth times (e-folding times) of 31 min and 79 min were obtained for the March and September cases, respectively.

The above simulations were run for a sufficiently long duration until the plasma bubble was well developed under the constant conditions. However, there was a disagreement between the simulations and observations. As mentioned already, most plasma bubble onsets were observed around the F-region sunset over the magnetic equator (Yokoyama et al., 2004). The initial conditions of the ambient ionosphere and seeding perturbation (e.g., Tsunoda and Ecklund, 2007) may contribute to the quick development of plasma bubbles, which will be the subject for future studies.

4 Conclusion

Ionosphere-thermosphere dynamics during equinox months (September 2004 and March 2005) was analyzed by using the meridional ionosonde chain at the longitude of 100° E. The analyses were conducted at three stations: two stations were situated near the magnetic conjugate points at Chiang Mai, Thailand (18.8° N, 98.9° E; 13.0° magnetic latitude) and Kototabang, Indonesia (0.2° S, 100.3° E; −10.0° magnetic latitude); and the third station was situated near the magnetic equator at Chumphon, Thailand (10.7° N, 99.4° E; 3.3° magnetic latitude). By using model calculations, vertical $\boldsymbol{E}\times\boldsymbol{B}$ drift velocities were inferred from the equatorial station, and the transequatorial component of the thermospheric wind was inferred from the conjugate pair of ionosondes. These ionosphere-thermosphere parameters were compared for the September and March equinoxes. An oscillation of the meridional winds with a period of approximately 7 h was dominant in both the periods, and its amplitude was significantly larger for the September equinox as compared to that of the March equinox.

During the time slot between the E-region and F-region sunsets, where most ionospheric plasma bubbles are initiated (Yokoyama et al., 2004), the northward meridional wind increased, and was larger at the September equinox (∼40 m/s) as compared to that of the March equinox (∼10 m/s). Equatorial irregularities are generally stronger in March as compared to those in September at the Indian to Western Pacific longitudes. Numerical simulations of plasma bubble developments incorporating the transequatorial neutral wind effect indicated that the growth time (e-folding time) of the bubble was halved when the wind velocity increased from 10 to 40 m/s. Thus, the larger meridional wind velocity and lower occurrence probability of equatorial irregularities in September compared with March were consistent with the hypothesis in which the transequatorial wind suppresses the Rayleigh-Taylor instability (Maruyama and Matuura, 1984).

Acknowledgements. We thank N. Hemmakorn and T. Boonchuk of King Mongkut's Institute of Technology Ladkrabang, Thailand and T. Komolmis of Chiang Mai University, Thailand for supporting the SEALION project. The research at the Naval Research Laboratory has been supported by the Office of Naval Research and by the National Aeronautics and Space Administration, USA.

Topical Editor K. Kauristie thanks two anonymous referees for their help in evaluating this paper.

References

Abdu, M. A.: Outstanding problems in the equatorial ionosphere-thermosphere electrodynamics relevant to spread F, J. Atmos. Solar-Terr. Phys., 63, 869–884, 2001.

Burke, W. J., Huang, C. Y., Gentile, L. C., and Bauer, L.: Seasonal-longitudinal variability of equatorial plasma bubbles, Ann. Geophys., 22, 3089–3098, 2004, http://www.ann-geophys.net/22/3089/2004/.

Forbes, J. M., Bruinsma, S. L., Miyoshi, Y., and Fujiwara, H.: A solar terminator wave in thermosphere neutral densities measured by the CHAMP satellite, Geophys. Res. Lett., 35, L14802, doi:10.1029/2008GL034075, 2008.

Herrero, F. A. and Spencer, N. W.: On the horizontal distribution of the equatorial thermospheric midnight temperature maximum and its seasonal variation, Geophys. Res. Lett., 9, 1179–1182, 1982.

Huba, J. D., Joyce, G., and Fedder, J. A.: Sami2 is Another Model of the Ionosphere (SAMI2): A new low-latitude ionosphere model, J. Geophys. Res., 105(A10), 23035–23053, 2000.

Huba, J. D., Joyce, G., Sazykin, S., Wolf, R., and Spiro, R.: Simulation study of penetration electric field effects on the low- to mid-latitude ionosphere, Geophys. Res. Lett., 32, L23101, doi:10.1029/2005GL024162, 2005.

Huba, J. D., Joyce, G., and Krall, J.: Three-dimensional equatorial spread F modeling, Geophys. Res. Lett., 35, L10102, doi:10.1029/2008GL033509, 2008.

Kelleher, R. F. and Röttger, J.: Equatorial spread-F irregularities observed at Nairobi and on the transequatorial path Lindau-Tsumeb, J. Atmos. Terr. Phys., 35, 1207–1211, 1973.

Kim, Y. H., Hong, S. S., and Weinberg, J. L.: Equatorial spread F found in 5577 Å and 6300 Å airglow observations from Hawaii, J. Geophys. Res., 107(A9), 1264, doi:10.1029/2001JA009232, 2002.

Krall, J., Huba, J. D., Joyce, G., and Zalesak, S. T.: Three-dimensional simulation of equatorial spread-F with meridional wind effects, Ann. Geophys, in press, 2009.

Makela, J. J., Ledvina, B. M., Kelley, M. C., and Kintner, P. M.: Analysis of the seasonal variations of equatorial plasma bubble

occurrence observed from Haleakala, Hawaii, Ann. Geophys., 22, 3109–3121, 2004, http://www.ann-geophys.net/22/3109/2004/.

Maruyama, T.: A diagnostic model for equatorial spread F, 1. Model description and application to electric field and neutral wind effects, J. Geophys. Res., 93(A12), 14611–14622, 1988.

Maruyama, T. and Kawamura, M.: Equatorial ionospheric disturbance observed through a transequatorial HF propagation experiment, Ann. Geophys., 24, 1401–1409, 2006, http://www.ann-geophys.net/24/1401/2006/.

Maruyama, T. and Matuura, N.: Longitudinal variability of annual changes in activity of equatorial spread F and plasma bubbles, J. Geophys. Res., 89(A12), 10903–10912, 1984.

Maruyama, T., Kawamura, M., Saito, S., Nozaki, K., Kato, H., Hemmakorn, N., Boonchuk, T., Komolmis, T., and Ha Duyen, C.: Low latitude ionosphere-thermosphere dynamics studies with inosonde chain in Southeast Asia, Ann. Geophys., 25, 1569–1577, 2007, http://www.ann-geophys.net/25/1569/2007/.

Maruyama, T., Saito, S., Kawamura, M., and Nozaki, K.: Thermospheric meridional winds as deduced from ionosonde chain at low and equatorial latitudes and their connection with midnight temperature maximum, J. Geophys. Res., 113, A09316, doi:10.1029/2008JA013031, 2008.

Mendillo, M., Baumgardner, J., Pi, X., Sultan, P. J., and Tsunoda, R.: Onset conditions for equatorial spread F, J. Geophys. Res., 97(A9), 13865–13876, 1992.

Mendillo, M., Meriwether, J., and Biondi, M.: Testing the thermospheric neutral wind suppression mechanism for day-to-day variability of equatorial spread F, J. Geophys. Res., 106(A3), 3655–3663, 2001.

Meriwether, J., Faivre, M., Fesen, C., Sherwood, P., and Veliz, O.: New results on equatorial thermospheric winds and the midnight temperature maximum, Ann. Geophys., 26, 447–466, 2008, http://www.ann-geophys.net/26/447/2008/.

Miyoshi, Y. and Fujiwara, H.: Gravity waves in the thermosphere simulated by a general circulation model, J. Geophys. Res., 113, D01101, doi:10.1029/2007JD008874, 2008.

Ogawa, T., Otsuka, Y., Shiokawa, K., Saito, A., and Nishioka, M.: Ionospheric disturbances over Indonesia and their possible association with atmospheric gravity waves from the troposphere, J. Meteor. Soc. Japan, 84A, 327–342, 2006.

Otsuka, Y., Shiokawa, K., and Ogawa, T.: Equatorial ionospheric scintillations and zonal irregularity drifts observed with closely-spaced GPS receivers in Indonesia, J. Meteor. Soc. Japan, 84A, 343–351, 2006.

Picone, J. M., Hedin, A. E., Drob, D. P., and Aikin, A. C.: NRLMSISE-00 empirical model of the atmosphere: Statistical comparisons and scientific issues, J. Geophys. Res., 107(A12), 1468, doi:10.1029/2002JA009430, 2002.

Ray, S. and DasGupta, A.: Geostationary L-band signal scintillation observations near the crest of equatorial anomaly in the Indian zone, J. Atmos. Solar-Terr. Phys., 69, 500–514, 2007.

Röttger, J.: The macro-scale structure of equatorial spread-F irregularities, J. Atmos. Terr. Phys., 38, 97–101, 1976.

Saito, S. and Maruyama, T.: Ionospheric height variations observed by ionosondes along magnetic meridian and plasma bubble onsets, Ann. Geophys., 24, 2991–2996, 2006, http://www.ann-geophys.net/24/2991/2006/.

Scherliess, L. and Fejer, B. G.: Radar and satellite global equatorial F region vertical drift model, J. Geophys. Res., 104(A4), 6829–6842, 1999.

Thampi, S. V., Ravindran, S., Pant, T. K., Devasia, C. V., Sreelatha, P., and Sridharan, R.: Deterministic prediction of post-sunset ESF based on the strength and asymmetry of EIA from ground based TEC measurements: Preliminary results, Geophys. Res. Lett., 33, L13103, doi:10.1029/2006GL026376, 2006.

Thampi, S. V., Ravindran, S., Pant, T. K., Devasia, C. V., and Sridharan, R.: Seasonal dependence of the "forecast parameter" based on the EIA characteristics for the prediction of Equatorial Spread F (ESF), Ann. Geophys., 26, 1751–1757, 2008, http://www.ann-geophys.net/26/1751/2008/.

Tsunoda, R. T.: Control of the seasonal and longitudinal occurrence of equatorial scintillations by the longitudinal gradient in integrated E region Pedersen conductivity, J. Geophys. Res., 90(A1), 447–456, 1985.

Tsunoda, R. T. and Ecklund, W. L.: On the post-sunset rise of the equatorial F layer and superposed upwellings and bubbles, Geophys. Res. Lett., 34, L04101, doi:10.1029/2006GL028832, 2007.

Valladares, C. E., Sheehan, R., and Villalobos, J.: A latitudinal network of GPS receivers dedicated to studies of equatorial spread F, Radio Sci., 39, RS1S23, doi:10.1029/2002RS002853, 2004a.

Valladares, C. E., Villalobos, J., Sheehan, R., and Hagan, M. P.: Latitudinal extension of low-latitude scintillations measured with a network of GPS receivers, Ann. Geophys., 22, 3155–3175, 2004b, http://www.ann-geophys.net/22/3155/2004/.

Yokoyama, T., Fukao, S., and Yamamoto, M.: Relationship of the onset of equatorial F region irregularities with the sunset terminator observed with the Equatorial Atmosphere Radar, Geophys. Res. Lett., 31, L24804, doi:10.1029/2004GL021529, 2004.

Zalesak, S. T. and Huba, J. D.: Effect of meridional winds on the development of equatorial spread-F, EOS Trans. AGU, 72, Spring Meet. Suppl., 211, 1991.